

Virtual Coil Concept for Improved Parallel MRI Employing Conjugate Symmetric Signals

Martin Blaimer,^{1,4*} Marcel Gutberlet,² Peter Kellman,³ Felix A. Breuer,⁴ Herbert Köstler,² and Mark A. Griswold¹

A new approach for utilizing conjugate k -space symmetry for improved parallel MRI performance is presented. By generating virtual coils containing conjugate symmetric k -space signals from actual coils, additional image- and coil-phase information can be incorporated into the reconstruction process for parallel acquisition techniques. In that way the reconstruction conditions are improved, resulting in less noise enhancement. In particular in combination with generalized autocalibrating partially parallel acquisitions (GRAPPA), the virtual coil concept represents a practical approach since no explicit spatial phase information is required. In addition, the influence of phase variations originating from the complex receiver coils as well as from the background is investigated. It is shown that there exist background phase distributions yielding an optimized pMRI reconstruction. Magn Reson Med 61:93–102, 2009. © 2008 Wiley-Liss, Inc.

Key words: parallel MRI; conjugate symmetry; SENSE; GRAPPA

Many strategies for reducing the scan time of MRI experiments work by collecting only a fraction of the data required for an artifact-free image. In the phase-constrained or partial-Fourier approach for Cartesian MRI, the k -space is sampled asymmetrically along the phase-encoding (PE) direction with full sampling density. While one-half of k -space is fully Fourier-encoded, only a portion of the other half of k -space is covered. Dedicated reconstruction algorithms recover the missing data by exploiting conjugate symmetry properties of k -space (1–3).

Alternative approaches for scan time reductions include the parallel MRI (pMRI) methods (for example (4–6)). The basic idea of Cartesian pMRI is to cover the entire span of k -space, but skip a fraction of the PE steps. In that way the Nyquist criterion is violated along the PE dimension, resulting in aliasing artifacts. Parallel MRI algorithms use spatial information inherent in an array of multiple receiver coils to either recover missing data in k -space or remove aliasing artifacts in the image domain. Cartesian sensitivity encoding (SENSE) (5) is a widespread image-domain pMRI technique that unfolds superimposed pixels by incorporating spatial coil sensitivity information. How-

ever, for nonideal coil configurations noise enhancement occurs as a result of ill-conditioning of the inverse solution. The noise enhancement varies within the field of view (FOV) and can be analytically described by the geometry factor (g -factor). In addition to SENSE, the k -space domain “generalized autocalibrating partially parallel acquisitions” (GRAPPA) (6) technique is widely used. In GRAPPA, missing k -space lines in a single coil are approximated by a linear combination of measured k -space lines from all coils. To calculate the reconstruction coefficients, additional Nyquist sampled k -space lines (autocalibration signal, ACS) have to be measured. Equivalent to SENSE, noise enhancement occurs depending on the coil sensitivity profiles. However, in contrast to SENSE an analytical prediction of the noise enhancement is not trivial for GRAPPA. Both SENSE and GRAPPA are successfully applied in daily clinical routine.

Several approaches for combining partial-Fourier acquisitions with parallel MRI have been presented to achieve additional acceleration (7–11).

In addition, methods have been proposed that employ conjugate symmetry for improved parallel MRI performance of undersampled full Fourier acquisitions. These methods use a priori knowledge of the image phase to reduce the number of unknowns in the pMRI reconstruction process (12–14), thereby decreasing the noise enhancement and allowing higher acceleration factors.

In this work we present an alternative method for utilizing conjugate symmetry properties of the k -space. By generating virtual coils containing conjugate symmetric k -space signals from actual coils, additional phase information is employed for improved reconstruction conditions. The influence of phase variations from complex coil sensitivities as well as from the background phase on the parallel MRI performance is investigated. The proposed virtual coil concept represents a practical approach for including conjugate symmetry properties in parallel MRI reconstruction processes. In addition, in combination with GRAPPA no explicit spatial knowledge of the background phase distribution or modifications of the reconstruction algorithm are required.

THEORY

Symmetric Complex-Conjugate Signals and Virtual Coils

The k -space signal received from a coil j represents the Fourier transform (FT) of the real spatial spin-density distribution $\rho(\mathbf{x})$ weighted by the spatial complex coil sensitivities $C_j(\mathbf{x})$ with \mathbf{x} representing a vector in image space. In normal imaging situations, an additional spatial background phase distribution $e^{i\varphi(\mathbf{x})}$ exists, depending on B_0 field homogeneity, RF pulse, and pulse sequence used for

¹Department of Radiology, University Hospitals of Cleveland and Case Western Reserve University, Cleveland, Ohio.

²Experimentelle MR Tomographie, Institut für Röntgendiagnostik, Universität Würzburg, Würzburg, Germany.

³Laboratory of Cardiac Energetics, National Institutes of Health, National Heart, Lung, and Blood Institute, Bethesda, Maryland.

⁴Research Center Magnetic Resonance Bavaria (MRB), Würzburg, Germany.

*Correspondence to: Martin Blaimer, Research Center Magnetic Resonance Bavaria (MRB), Am Hubland, 97074 Würzburg, Germany. E-mail: blaimer@mrbavaria.de

Received 29 August 2007; revised 17 January 2008; accepted 13 March 2008.

DOI 10.1002/mrm.21652

Published online in Wiley InterScience (www.interscience.wiley.com).

imaging. The background phase can be combined with the coil sensitivities to generate effective coil sensitivities $D_j(\mathbf{x}) = e^{i\varphi(\mathbf{x})} \cdot C_j(\mathbf{x})$, and thus the received signal can be formulated as:

$$S_j(\mathbf{k}) = \int d\mathbf{x} \cdot \rho(\mathbf{x}) \cdot e^{i\varphi(\mathbf{x})} \cdot C_j(\mathbf{x}) \cdot e^{-i\mathbf{k}\mathbf{x}} = \text{FT}[\rho(\mathbf{x}) \cdot D_j(\mathbf{x})]. \quad [1]$$

Here, \mathbf{k} represents a vector in k -space. The symmetric complex-conjugate signal has the form:

$$\begin{aligned} S_j^*(-\mathbf{k}) &= \int d\mathbf{x} \cdot \rho(\mathbf{x}) \cdot e^{-i\varphi(\mathbf{x})} \cdot C_j^*(\mathbf{x}) \cdot e^{i(-\mathbf{k})\mathbf{x}} \\ &= \text{FT}[\rho(\mathbf{x}) \cdot D_j^*(\mathbf{x})], \quad [2] \end{aligned}$$

with $*$ denoting the complex-conjugate operation. The signal from Eq. [2] can be interpreted as signal received with a virtual coil having the complex sensitivity distribution $D_j^*(\mathbf{x}) = e^{-i\varphi(\mathbf{x})} \cdot C_j^*(\mathbf{x})$. The signals $S_j(\mathbf{k})$ and $S_j^*(-\mathbf{k})$ are equal only for the case of effective coil sensitivities without imaginary part (equivalent to $D_j^*(\mathbf{x}) = D_j(\mathbf{x})$). However, the coil sensitivities are complex under normal imaging situations, yielding $S_j(\mathbf{k}) \neq S_j^*(-\mathbf{k})$.

Although the magnitude sensitivity from a virtual coil is the same as from an actual coil, the phase is different and therefore provides additional encoding power. For example, Hajnal et al. (15) have shown that both sensitivity-magnitude and sensitivity-phase contribute to the array encoding power.

Data Reconstruction Using GRAPPA

In modern GRAPPA implementations (16–18), missing data points in a single coil j are reconstructed by a linear combination of a kernel of acquired data points from all N coils:

$$S_j(\mathbf{k}_a) = \sum_{l=1}^N \sum_{b=1}^{N_b} w(j,a,l,b) \cdot S_l(\mathbf{k}_b) \quad [3]$$

Here, \mathbf{k}_a is the location of a missing data point, \mathbf{k}_b are the locations of the surrounding acquired points from both PE and the readout direction, and $w(j,a,l,b)$ are the weighting coefficients.

Typically, a kernel of a few data points (e.g., kernel size $N_b = 20$) leads to acceptable results. However, the search for an optimized size of the GRAPPA reconstruction kernel is still an active field of research (17,19,20).

In this work, additional phase information is incorporated in the reconstruction process by extending the conventional GRAPPA kernel using complex-conjugate symmetric signals:

$$S_j(\mathbf{k}_a) = \sum_{l=1}^N \sum_{b=1}^{N_b} \tilde{w}(j,a,l,b) \cdot S_l(\mathbf{k}_b) + \sum_{l=1}^N \sum_{b=1}^{N_b} \tilde{\tilde{w}}(j,a,l,b) \cdot S_l^*(-\mathbf{k}_b) \quad [4]$$

A practical approach for incorporating the complex-conjugate symmetric signals is the virtual coil concept described in the following section.

Using Eq. [2] and a phased array with N elements, additional signal from a virtual coil can be generated from an actual coil j in the following way:

$$S_{j+N}(\mathbf{k}) = S_j^*(-\mathbf{k}), \quad j = 1, \dots, N. \quad [5]$$

The resulting dataset consists of signals virtually received with $2 \cdot N$ coils.

By inserting Eq. [5] into Eq. [4], a conventional GRAPPA reconstruction can be formed, now summing over $2 \cdot N$ channels:

$$S_j(\mathbf{k}_a) = \sum_{l=1}^{2 \cdot N} \sum_{b=1}^{N_b} \tilde{w}(j,a,l,b) \cdot S_l(\mathbf{k}_b)$$

In the following the individual reconstruction steps for GRAPPA using the virtual coil concept are described. In a first step, virtual coils are formed for both ACS and undersampled data according to Eq. [5]. In the second step a standard GRAPPA reconstruction is performed and the resulting images are combined using a sum-of-squares combination, for example. For the reconstruction process, no explicit spatial phase maps and no modifications of the GRAPPA algorithm are required.

To provide consistent phase information, the ACS and undersampled data have to be acquired with the same sequence parameters so that $D_j^{ACS}(\mathbf{x}) = D_j^{Undersampled}(\mathbf{x})$. Thus, a variable-density (VD) acquisition scheme as proposed in the original GRAPPA (6) approach or a time-interleaved acquisition as used in many dynamic applications (21–24) work well with the virtual coil concept.

Data Reconstruction Using Cartesian SENSE

The virtual coil concept can also be employed for Cartesian SENSE. Starting from Eqs. [1] and [2], single coil images $a_j(\mathbf{x})$ and $b_j(\mathbf{x})$ are generated by inverse Fourier-transform of the acquired and the virtual signals:

$$\begin{aligned} a_j(\mathbf{x}) &= \text{FT}^{-1}(S_j(\mathbf{k})) = \rho(\mathbf{x}) \cdot D_j(\mathbf{x}) \\ b_j(\mathbf{x}) &= \text{FT}^{-1}(S_j^*(-\mathbf{k})) = \rho(\mathbf{x}) \cdot D_j^*(\mathbf{x}) \quad [6] \end{aligned}$$

Uniform Cartesian undersampling of rate R that is symmetric around $\mathbf{k} = 0$ results in aliased reconstructed images $a_j(\mathbf{x})$ and $b_j(\mathbf{x})$ that may be written as:

$$\begin{aligned} a_j(x,y) &= \sum_{n=0}^{R-1} \rho(x,y - n\text{FOV}/R) \cdot D_j(x,y - n\text{FOV}/R) \\ b_j(x,y) &= \sum_{n=0}^{R-1} \rho(x,y - n\text{FOV}/R) \cdot D_j^*(x,y - n\text{FOV}/R) \quad [7] \end{aligned}$$

By using measured single coil images $a_j(\mathbf{x})$ and additional virtual coil images $b_j(\mathbf{x})$, an extended Cartesian SENSE equation is built up in the following way:

$$\begin{bmatrix} a_1(x,y) \\ \vdots \\ a_N(x,y) \\ b_1(x,y) \\ \vdots \\ b_N(x,y) \end{bmatrix} = \begin{bmatrix} D_1(x,y) & \cdots & D_1(x,y - (R-1)FOV/R) \\ \vdots & & \vdots \\ D_N(x,y) & \cdots & D_N(x,y - (R-1)FOV/R) \\ D_1^*(x,y) & \cdots & D_1^*(x,y - (R-1)FOV/R) \\ \vdots & & \vdots \\ D_N^*(x,y) & \cdots & D_N^*(x,y - (R-1)FOV/R) \end{bmatrix} \times \begin{bmatrix} \rho(x,y) \\ \vdots \\ \rho(x,y - (R-1)FOV/R) \end{bmatrix}$$

Or in short form:

$$\begin{bmatrix} \mathbf{a} \\ \mathbf{b} \end{bmatrix} = \begin{bmatrix} \mathbf{D} \\ \mathbf{D}^* \end{bmatrix} \cdot \boldsymbol{\rho} \quad [8]$$

Equivalent to Cartesian SENSE, the unaliased object is recovered by solving Eq. [8] for the vector $\boldsymbol{\rho}$.

If $D_j(\mathbf{x})$ and $D_j^*(\mathbf{x})$ are linear independent, the conditioning for the inversion of the extended coil sensitivity matrix $\begin{bmatrix} \mathbf{D} \\ \mathbf{D}^* \end{bmatrix}$ is improved resulting in a reduced g-factor and thus less noise enhancement as compared to standard Cartesian SENSE. Neglecting noise correlations, the g-factor can be calculated equivalently as presented by Pruessmann et al. (5):

$$g_i = \sqrt{((\mathbf{E}^H \mathbf{E})^{-1})_{i,i} (\mathbf{E}^H \mathbf{E})_{i,i}} \quad \text{with } \mathbf{E} = \begin{bmatrix} \mathbf{D} \\ \mathbf{D}^* \end{bmatrix} \quad [9]$$

Prior to data reconstruction using SENSE, spatial knowledge about coil sensitivities and background phase is required. Several approaches have been proposed for obtaining low-resolution coil sensitivity maps and background phase information including a VD acquisition scheme or the combination of VD acquisition for phase estimation with a prescan for coil sensitivity measurement. More details can be found in Refs. (11) and (14), for example. In dynamic imaging, high-resolution coil sensitivity information and phase maps could be obtained by using a time-interleaved acquisition scheme and combining adjacent timeframes.

Influence of Background Phase

It can be seen from Eqs. [1] and [2] that the background phase is included in $D_j(\mathbf{x})$ and $D_j^*(\mathbf{x})$, and thus contributes to the encoding power. To provide an intuitive comprehension, a simple example is described in the following.

Consider a single coil with homogeneous uniform sensitivity $C_1(\mathbf{x}) = 1$ and undersampling of rate $R = 2$. If there is no background phase, Eq. [8] cannot be solved because

measured and virtual image provide the same information. However, if there exists a background phase distribution, so that there is a phase difference of $\pi/2$ between the aliased pixels, Eq. [8] can be written as:

$$\begin{bmatrix} a_1(x,y) \\ b_1(x,y) \end{bmatrix} = \begin{bmatrix} 1 & i \\ 1 & -i \end{bmatrix} \begin{bmatrix} \rho(x,y) \\ \rho(x,y - FOV/2) \end{bmatrix}. \quad [10]$$

This equation can be solved resulting in a perfect separation of the aliased pixels without noise enhancement ($g = 1$) by incorporating the a priori background phase information.

For the specific example of a single homogeneous coil and undersampling of rate $R = 2$, the g-factor can be analytically described as a function of the phase difference $\Delta\varphi$ between the two superimposed pixels (see Appendix):

$$g(\Delta\varphi) = 1/\sin(\Delta\varphi) \quad [11]$$

Equation [11] characterizes both cases described above: 1) for $\Delta\varphi = 0$ the superimposed pixels cannot be separated corresponding to a g-factor toward infinity, and 2) for $\Delta\varphi = \pi/2$ the superimposed pixels are perfectly separable corresponding to a g-factor of $g = 1$.

There are several ways of introducing a linear background phase, including shifting the sampling scheme, varying the phase profile of the receiver coil, or modifying shim settings.

This concept can be extended for multicoil arrays and higher acceleration factors. For each experimental setup there should exist fixed background phase distributions that complement the coil sensitivity encoding yielding a minimized g-factor. In contrast to a single homogenous coil, the phase distribution is expected to differ from a linear phase since the phase variations of the receiver coils have to be taken into account. When the complex coil sensitivities are known, the optimal phase difference between superimposed pixels can be determined. To this end, the minimum g-factor may be found using a simplex search method (with the g-factor calculated using Eq. [9]). It should be noted that there exist multiple optimized phase distributions yielding the same result since phase differences between superimposed pixels are calculated. Therefore, the final phase distribution depends on initial estimates and constraints.

MATERIALS AND METHODS

All imaging studies were performed on clinical 1.5T scanners (Siemens Medical Solutions, Erlangen, Germany). Informed consent was obtained from normal volunteers before each in vivo study. All computer simulations and image reconstructions were performed using the MatLab programming environment (MathWorks, Natick, MA). For the GRAPPA reconstructions, the ACS lines were used for calibration only and have not been integrated into the final reconstruction.

Computer Simulations

In a first step, the proposed virtual coil concept was investigated by computer simulations. To this end, Biot-Savart

calculations were performed to derive spatial sensitivity maps for an axial slice within an eight-channel head array. A circular disk, representing an object with constant real spin-density distribution, was multiplied by the sensitivity maps. An additional linear phase along the PE direction was applied to the object to simulate a background phase variation. The phase values were chosen to range from $-\pi$ to π radians. The resulting images were Fourier-transformed and complex Gaussian noise was added to obtain the simulated k -space data. Geometry factor calculations and Cartesian SENSE reconstructions (acceleration factor $R = 4$) were performed with and without virtual coil concept using sensitivity information from the Biot-Savart calculations. In addition, corresponding GRAPPA reconstructions (acceleration factor $R = 4$) with and without virtual coil concept were performed. For the calibration process, 24 ACS lines were used. The resulting single-coil images were combined using array correlation statistics (25).

For the simulated eight-channel array an optimized background phase distribution yielding a minimized g -factor was determined by using a simplex search algorithm (26). This algorithm finds the minimum of a scalar function (in this case the g -factor in Eq. [9]) using a derivative-free method. As an initial estimate, a linear phase along the PE direction was applied, so that the initial background phase difference between superimposed pixels was $\pi/2$.

Phantom MRI Experiment

A phantom experiment was performed using a 12-channel head coil array (Siemens Medical Solutions). For imaging, a T_1 -weighted spin-echo sequence was used (parameters: TE = 12 ms, TR = 450 ms, FOV = 173×230 mm², slice thickness = 5 mm, matrix = 173×256). The fully encoded dataset was reduced by removing corresponding PE lines in order to mimic an undersampling factor of $R = 4$. GRAPPA reconstructions were performed with and without virtual coil concept using 32 ACS lines for calibration. In addition to the symmetric sampling scheme around $k = 0$, the effect of a shifted sampling scheme was investigated since it was expected to improve the reconstruction quality according to Ref. (14). The shift was chosen to be Δk corresponding to a linear phase variation of 2π over the FOV in object space according to the Fourier-shift theorem. The reconstruction quality was evaluated by artifact-plus-noise power, which was computed by the mean squared absolute difference between reconstructed and reference image (acquired with full k -space) normalized by the mean squared absolute pixel intensities of the reference.

In Vivo Single-Coil MRI Experiment

An in vivo experiment was performed using a single-channel head coil (Siemens Medical Solutions) for signal reception.

A spin-echo sequence was used to acquire a fully Fourier-encoded image. The sequence parameters were TE = 15 ms, TR = 450 ms, FOV = 235×235 mm², slice thickness = 6 mm, matrix = 320×512 .

Datasets corresponding to signals acquired with shifted sampling schemes were generated by applying linear phase profiles to the artifact-free image followed by a Fourier transform. Undersampled ($R = 2$) datasets were obtained by removing corresponding k -space lines.

For each individual shifted sampling scheme, an additional virtual coil was generated. Both Cartesian SENSE and GRAPPA reconstructions were performed. For SENSE, only the phase information from the fully encoded image was used for reconstruction assuming a homogeneous magnitude sensitivity of the receiver coil. Phase fluctuations due to noise were smoothed by applying a filter with uniform smoothing kernel of size 3×3 . It should be noted that this particular filter might not be optimal for this purpose. For the GRAPPA reconstructions, 32 ACS lines were used for calibration.

In addition, a half-Fourier reconstruction was compared to a virtual coil reconstruction using GRAPPA. To that end, 16 lines from central k -space were used to obtain a low-resolution phase map for an iterative half-Fourier reconstruction. The same 16 lines from central k -space were used as ACS for GRAPPA so that the same number of k -space lines were included for the individual reconstructions.

In Vivo Multicoil MRI Experiments

An accelerated in vivo abdominal MRI experiment was performed. For signal reception, in total 12 channels from the vendor-supplied body- and spine-arrays were combined. A balanced steady-state free precession sequence (TrueFISP) with a VD acquisition scheme was used for acquiring axial slices. The sequence parameters were: TE = 2.0 ms, TR = 4.0 ms, flip angle = 70° , FOV = 213×310 mm², slice thickness = 5 mm, matrix = 176×256 , acceleration factor $R = 3$. GRAPPA reconstructions with and without virtual coils were performed using 24 ACS lines for calibration.

Free-breathing dynamic cardiac imaging studies were performed using an eight-channel cardiac array (Nova Medical, Wilmington, MA) for signal reception. A TrueFISP sequence with a time-interleaved PE scheme was used for data acquisition. The sequence parameters were: TE = 1.43 ms, TR = 2.86 ms, flip angle = 50° , FOV = 270×360 mm², slice thickness = 6 mm, matrix = 92×192 . Using a 4-fold acceleration ($R = 4$), 23 k -space lines were collected per frame, corresponding to a temporal resolution of 66 ms. Analogous to conventional TGRAPPA (23), 16 adjacent timeframes were assembled to obtain the ACS for an individual timeframe.

RESULTS

Computer Simulations

Figure 1 shows results from the computer simulation. Geometry factor maps (Fig. 1, top row), SENSE reconstructions (Fig. 1, middle row), and GRAPPA reconstructions (Fig. 1, bottom row) are presented for an acceleration factor of $R = 4$. Three scenarios were investigated: 1) conventional reconstructions without virtual coils (Fig. 1, left column); 2) reconstructions using virtual coils without a background phase distribution (Fig. 1, middle columns);

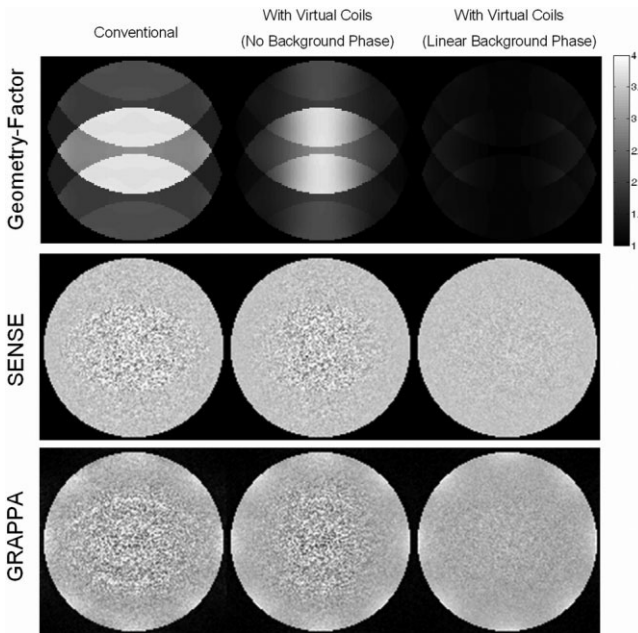


FIG. 1. Results from the computer simulation of an eight-channel head coil array using an undersampling factor of $R = 4$. Geometry factor maps (top row), SENSE reconstructions (middle row), and GRAPPA reconstructions (bottom row) are presented for three set-ups: 1) conventional reconstructions (left column); 2) reconstructions using the virtual coil concept without background phase (middle column); and 3) reconstructions using the virtual coil concept with additional linear background phase along the phase-encoding direction (right column).

and 3) reconstructions using virtual coils with a linear background phase along the PE direction. In Table 1, mean and maximum g-factors for all three scenarios are presented.

The conventional setup exhibits the largest g-factor values throughout the FOV. By including the virtual coils, reduced g-factors can be observed even when there is no background phase. The lateral coils provide sufficient phase variations along the PE direction yielding improved reconstruction conditions on the side of the FOV. However, the central part of the FOV still exhibits large g-factors. A significant reduction of the g-factors can be observed throughout the entire FOV for the case of an additional linear background phase. For this particular scenario the phase difference of superimposed pixels is close to $\pi/2$, resulting in nearly optimal g-factors.

Table 1
Mean and Maximum g-Factors from the Computer Simulation

	Conventional	With Virtual Coils (No Background Phase)	With Virtual Coils (Linear Background Phase)
Mean g-factor	2.07	1.77	1.12
Max g-factor	3.80	3.76	1.56

Mean and maximum g-factors from the computer simulation of an 8-channel head array and acceleration factor of $R = 4$. Three scenarios were investigated: 1) conventional reconstructions (left column), 2) reconstructions using virtual coils without background phase (middle column), and 3) reconstructions using virtual coils and an additional linear background phase along the phase-encoding direction (right column).

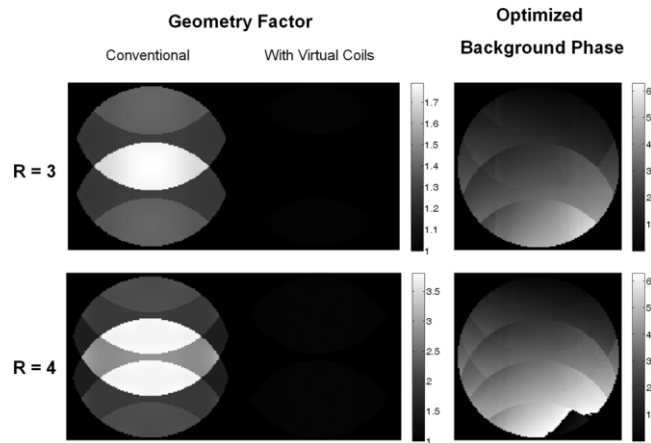


FIG. 2. Optimized background phase distributions (right column) for a simulated eight-channel head coil array using acceleration factors $R = 3$ (top row) and $R = 4$ (bottom row). The phase values shown range from 0 to 2π . With the optimized background phase distributions a significantly reduced g-factor is observed ($g < 1.1$) for the reconstructions with virtual coils (middle column) as compared to conventional reconstructions without virtual coils (left column).

A further reduction of the g-factors can be observed for optimized background phase distributions. Corresponding simulation results are shown in Fig. 2. Even for acceleration factors of $R = 3$ and $R = 4$, the optimized phase distributions (Fig. 2, right column) yield very low g-factors with values $g < 1.1$ (see Table 2). It should be mentioned that these results are simulated and it remains to be seen if such phase distributions can be realized in actual imaging situations.

Phantom MRI Experiment

Results from a phantom experiment using a multicoil array are presented in Fig. 3. GRAPPA reconstructions (acceleration factor $R = 4$) without (Fig. 3b) and with virtual coils using a symmetric sampling around $k = 0$ (Fig. 3c) are shown. In addition, a GRAPPA reconstruction with virtual coils is presented in Fig. 3d. Here the sampling scheme was shifted by Δk along the PE direction corresponding to a linear background phase in object space. The artifact-plus-noise powers for the reconstructed images are listed in Table 3. These results confirm the findings of the computer simulations demonstrating an improved reconstruction quality of the virtual coil concept, in particular in the presence of a beneficial background phase.

Table 2
Effects of the Simulated Optimized Background Phase

Acceleration	Conventional		Virtual Coils + Optimized Background Phase	
	g_{mean}	g_{max}	g_{mean}	g_{max}
R = 3	1.28	1.79	1.00	1.01
R = 4	2.07	3.80	1.04	1.08

Effects of the simulated optimized background phase using acceleration factors of R = 3 and R = 4. Compared to the conventional reconstructions without, the g-factors are significantly reduced by applying an optimized background phase distribution and using virtual coils for data reconstruction.

In Vivo Single-Coil MRI Experiment

In Fig. 4 the results from a spin-echo experiment are shown. A homogeneous single-channel head coil was used for signal reception. Cartesian SENSE and GRAPPA reconstructions (acceleration factor R = 2) employing an additional virtual coil are presented for symmetric sampling around $k = 0$ (shift S = 0) and sampling shifted by $S = \Delta k/2$ along the PE direction.

Improved image quality can be observed when the sampling scheme is shifted by $\Delta k/2$. In the image domain, this corresponds to a linear background phase yielding a $\pi/2$ phase difference between the superimposed pixels (see Fig. 4a, bottom row).

For this particular case the virtual coil concept works analogous to a half-Fourier reconstruction in the sense that a priori phase information is used for image reconstruction. This can also be described in the k -space domain. For a real object and shifted sampling with $S = \Delta k/2$, the conjugate symmetric signals (e.g., from lines [..., -2.5, -0.5, 1.5, 3.5, ...]) from the virtual coil fall between the measured signals (corresponding to the lines [..., -3.5, -1.5, 0.5, 2.5, ...]) from the actual coil and are used to fill in the missing signals (see Fig. 4b, bottom, right).

However, the appearance of the remaining artifacts indicates nonideal imaging conditions. In principle, the ar-

tifacts can be divided into two categories, 1) artifacts due to an insufficient phase difference between superimposed pixels, and 2) artifacts due to inaccurate phase information.

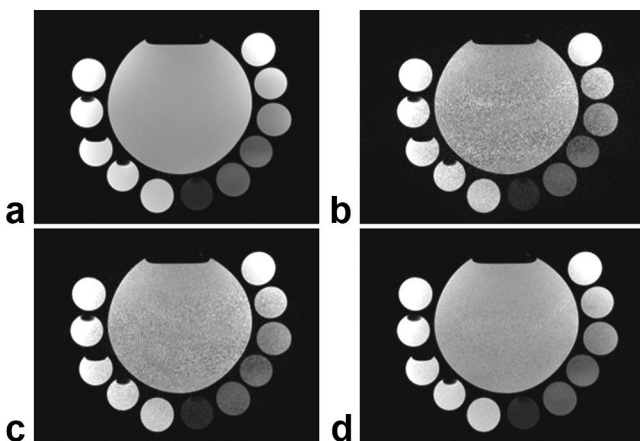


FIG. 3. Results from a phantom spin-echo experiment using an acceleration factor R = 4 and a 12-channel array for signal reception. Illustrated are a fully sampled reference image (a), a conventional GRAPPA reconstruction without virtual coil concept (b), a GRAPPA reconstruction with virtual coils, symmetric sampling around $k = 0$ (c), and GRAPPA reconstruction with virtual coils and sampling scheme shifted by Δk along the PE direction (d).

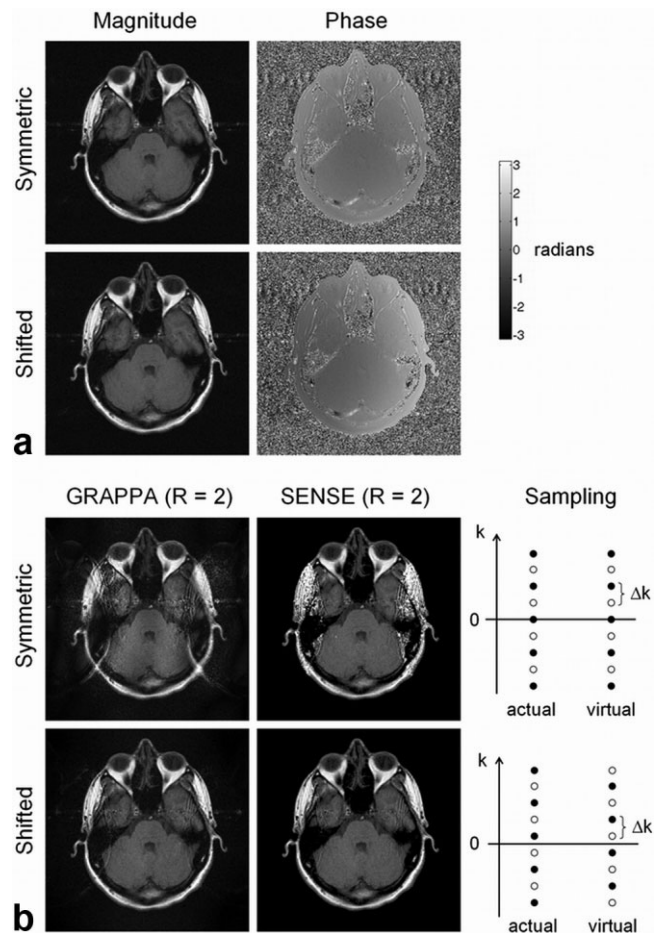


FIG. 4. Results from the single-coil spin-echo experiment. **a:** Magnitude and phase images from the fully Fourier-encoded reference image are presented for symmetric sampling around $k = 0$ (top row) and a sampling scheme shifted by $S = \Delta k/2$ along the PE direction (bottom row). **b:** GRAPPA (left column) and SENSE reconstructions (middle column) for rate R = 2 undersampled data are shown for symmetric (S = 0, top row) and shifted sampling (S = $\Delta k/2$, bottom row). The corresponding sampling schemes are presented in the right column with black and white circles representing measured and not-measured k -space lines, respectively. For the case of a shifted sampling, the measured signals from the virtual coils fall in between the measured signals from the actual coils.

Table 3
Artifact-plus-Noise Power (AP) from the Multicoil Phantom Experiment

	Conventional	With Virtual Coils (Symmetric Sampling)	With Virtual Coils (Shifted Sampling)
AP	$7.14 \cdot 10^{-3}$	$3.68 \cdot 10^{-3}$	$1.10 \cdot 10^{-3}$

Artifact-plus-noise power (AP) from the multicoil phantom experiment for a conventional GRAPPA reconstruction and reconstructions with virtual coils using symmetric and shifted sampling schemes.

The reconstructions with $S = 0$ exhibit noise enhancement and remaining aliasing artifacts originating from insufficient background phase variation (Fig. 4b, top row) and can be assigned to artifacts of category 1. The reconstructions with $S = \Delta k/2$ are significantly improved but exhibit remaining aliasing artifacts due to inaccurate phase information (Fig. 4b, bottom row) and can be assigned to artifacts of category 2. Although the phase information is available in high resolution, phase jumps are not captured by the GRAPPA reconstruction kernel, which inherently acts as a low-pass filter due to the limited kernel size. For SENSE, a smoothing filter was applied to the phase information in order to remove phase fluctuations resulting in signal dropouts and remaining aliasing artifacts at the phase jump locations.

In Fig. 5 a comparison between a half-Fourier and a virtual coil reconstruction using GRAPPA is presented. The difference images between the individual reconstructions and the fully Fourier-encoded image indicate similar image quality and show the different reconstruction errors for both approaches. In the half-Fourier reconstruction, errors appear as blurring at the locations where the phase information cannot be estimated accurately. In this particular example, locations with fast phase variations are the

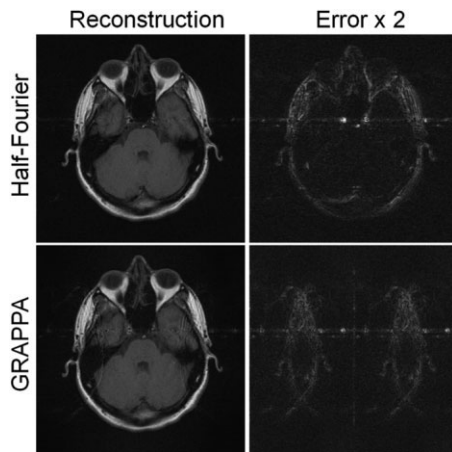


FIG. 5. Comparison between a half-Fourier approach (top row) and GRAPPA with virtual coil concept (bottom row) using a single coil for signal reception. The difference images between the individual reconstructions and the fully Fourier-encoded image indicate the reconstruction errors for both approaches (right column). Please note that the difference images are multiplied by a factor of two.

critical locations for accurate phase estimations. In contrast, the errors by the virtual coil reconstruction appear as remaining aliasing artifacts. These artifacts are typical errors known from parallel MRI reconstruction and occur only in the regions where pixel overlap.

In Vivo Multicoil MRI Experiments

Figure 6 shows GRAPPA reconstructions ($R = 3$) from an axial abdominal slice. The reconstructions employing virtual coils (Fig. 6b) exhibit less noise enhancement compared to the conventional GRAPPA reconstructions (Fig. 6a). In particular, in the central part of the FOV and near the kidneys the images reconstructed with additional virtual coils shows improved image quality.

In Fig. 7 the results from an accelerated ($R = 4$) free-breathing dynamic cardiac MRI experiment are presented. Representative images from two cardiac phases are shown. Compared to conventional TGRAPPA results (Fig. 7, top row), the reconstructions with virtual coil concept exhibit less noise enhancement and reveal more details, in particular in the heart and lung tissue (Fig. 7, bottom row). In this example the reconstruction quality is significantly improved when using the virtual coil concept, although the timeframes were acquired using different phase-encoding offsets. These results indicate that phase variations originating from the complex coil sensitivities significantly contribute to the encoding in this example.

DISCUSSION

In this work, additional encoding power from virtual coils was employed for improved image quality in Cartesian parallel MRI experiments. The presented approach is analogous to the phase-constrained parallel MRI reconstruction method proposed by Willig-Onwuachi et al. (14). However, while the phase-constrained method reduces the number of unknown variables, the proposed approach adds additional equations to the reconstruction matrix.

The main advantage of our approach is the easy implementation for improved parallel MRI performance without requiring modifications of the reconstruction algorithms. In contrast to previous approaches, the virtual coil concept allows one to include conjugate symmetry properties for both Cartesian SENSE and GRAPPA reconstructions. In particular, in combination with GRAPPA this approach represents a practical approach that does not require explicit knowledge of the spatial background phase. Effec-

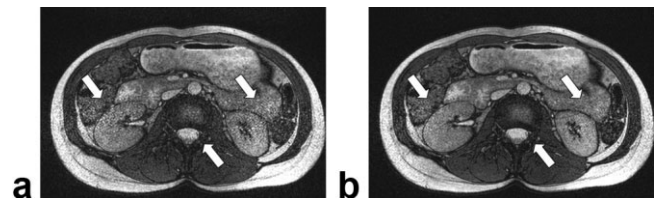


FIG. 6. Results from an accelerated ($R = 3$) abdominal experiment using an array of 12 receiver coils. Compared to the conventional GRAPPA reconstruction (a) the reconstruction with additional virtual coils (b) yields less noise enhancement, in particular in the central FOV and near the kidneys (see arrows).

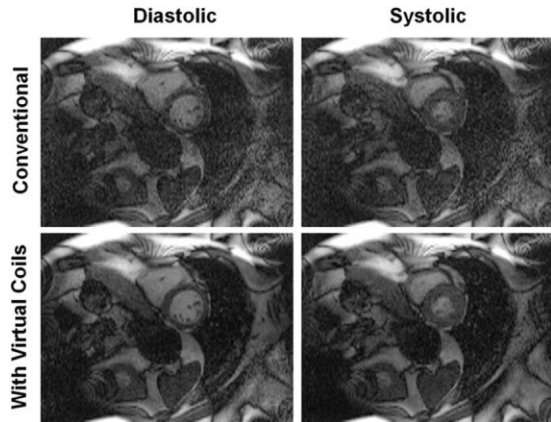


FIG. 7. Results from an accelerated ($R = 4$) time-interleaved free-breathing dynamic cardiac experiment using an eight-channel cardiac array for signal reception. Representative images from diastolic (left column) and systolic (right column) cardiac phases are shown. The two cardiac phases were acquired with different phase-encoding offsets. Image reconstruction was performed with conventional TGRAPPA (top row) and TGRAPPA using the virtual coil concept (bottom row). The temporal resolution in this experiment was 66 ms per timeframe corresponding to a frame rate of 15 frames per second.

tively, the standard GRAPPA reconstruction kernel is extended by complex-conjugate source signals from the mirrored k -space region and provides additional encoding power. In this work we have presented improved GRAPPA results from in vivo imaging with a VD acquisition and also from in vivo dynamic imaging using a time-interleaved acquisition.

For the case of a single homogeneous receive coil, a linear phase variation by π over the FOV enables the reconstruction of rate $R = 2$ undersampled datasets by using the virtual coil concept. For this particular case, the data reconstruction works similar to half-Fourier reconstruction in the sense that complex-conjugate signals from the mirrored k -space region are used to fill in missing signals. Differences to half-Fourier approaches are the appearance of artifacts due to insufficient phase variations or inaccurate spatial phase information. In this work, the phase variation was introduced by shifting the sampling scheme by $\Delta k/2$.

Equivalently, shifting the sampling scheme by Δk significantly improved the image quality for rate $R = 4$ undersampled reconstructions in combination with symmetric head-coil arrays used in this work. However, phase variations arising from the complex coil sensitivities have to be taken into account when further improvements in reconstruction quality are required. For example, linear phase variations in a single coil can be represented as an additional shift in k -space. In general, there exist fixed background phase distributions yielding optimal reconstruction conditions for each experimental setup. It has been demonstrated that an optimized background phase difference between the superimposed pixels can be determined by solving for a minimal g-factor. In this work, a simplex search algorithm was used for finding these background phase distributions. Although there might be a faster and

more robust approach for solving this problem, the simulation results demonstrate that significant g-factor reductions could be obtained by applying the optimized background phase distributions that depend on coil arrangement, acceleration factor, and object shape. So far, these optimized phase distributions have not been applied in actual experiments. It remains to be seen if there are feasible ways of realizing such background phase distributions in multicoil imaging situations. A possible approach could include the selective RF excitation by transmit arrays, for example.

It should be noted that an optimized background phase is also expected to result in improved performance of phase-constrained reconstructions or equivalent approaches that include image phase in the reconstruction process.

The requirements for an improved reconstruction performance as compared with traditional parallel imaging methods are 1) consistent phase information between reference (or ACS) and undersampled data, and 2) the existence and accurate knowledge of spatial phase variations originating from either the complex image or the coil sensitivity profiles.

If there is a phase information mismatch between reference and undersampled data, a virtual coil reconstruction might result in inferior image quality as conventional pMRI approaches exhibiting image artifacts. Therefore, a VD or a time-interleaved acquisition scheme might be preferable because the same sequence parameters are used and the acquisition of reference and undersampled data is in close temporal proximity.

In addition, an accurate knowledge about the background and coil sensitivity phase is required. In particular, phase jumps in the image are problematic for the reconstruction process. In that case, high-resolution phase information is required for an artifact-free reconstruction. For example, in TSENSE (22) and Auto-SENSE (24) a full spatial resolution image is obtained by merging adjacent time-interleaved acquisitions. Although motion can lead to temporal blurring when merging adjacent timeframes, high-resolution phase information is in principle available. Also, in TGRAPPA a fully Fourier-encoded ACS dataset is available corresponding to an image with full spatial resolution. However, the GRAPPA reconstruction process inherently smoothes the spatial phase information. This can be explained by the limited number of surrounding source points used for the reconstruction of a missing data point (i.e., the reconstruction kernel is limited in size).

In addition, the time-interleaved acquisition used for dynamic applications leads to a varying background phase from one time frame to the next since the k -space sampling scheme is shifted. Therefore, the g-factor distribution and thus the noise appearance are time-varying after image reconstruction. However, in the TGRAPPA example presented in this work (see Fig. 7) the overall image quality is significantly improved as compared with conventional reconstructions and the time-varying noise distribution is visually difficult to detect.

The results presented in this work were demonstrated for Cartesian MRI experiments with uniform undersampling. To introduce a background phase, the PE lines were

shifted. However, it should be noted that GRAPPA is more flexible in choosing the PE lines than Cartesian SENSE. Therefore, instead of shifting the sampling scheme alternative sampling patterns could be applied. For example, for GRAPPA with $R = 2$ improved reconstructions are expected by acquiring the odd lines in the first half of k -space and the even lines in the second half of k -space.

In principle, the virtual coil concept can also be applied to 3D imaging and experiments with non-Cartesian trajectories like projection reconstruction (PR), for example. As stated above, it might be beneficial to use modified PR sequences so that the projection angle is slightly modified during central readout. In that case the signals from the virtual coils would fall between the actually acquired signals. Although this approach is expected to result in improved reconstruction quality, more detailed investigations are necessary.

However, the cost for the improved reconstruction quality is an increased computation time, as the number of channels is doubled.

CONCLUSIONS

Incorporating complex-conjugate signals from the mirrored k -space region leads to an improved reconstruction quality in parallel MRI experiments. In this work, the symmetric complex-conjugate signals were employed by introducing a virtual coil concept. In particular, in combination with standard GRAPPA the virtual coil concept represents an elegant approach since no explicit knowledge of the background phase and no modifications of the reconstruction algorithm are required. Improved reconstruction quality has been demonstrated in both static and dynamic in vivo MRI experiments. In addition, it has been shown that both background- and coil-phase variations influence the reconstruction quality and that there exist fixed background phase distributions, yielding a minimized noise enhancement.

ACKNOWLEDGMENT

The authors thank Siemens Medical Solutions for their support.

APPENDIX

By incorporating symmetric complex-conjugate signals, rate $R = 2$ undersampled datasets can be reconstructed using a single coil.

In the following, the g -factor dependent on the background phase difference $\Delta\varphi$ between two superimposed pixels is derived for the case of a single homogeneous receiver coil and an undersampling rate $R = 2$. Starting from Eq. [8], an extended Cartesian SENSE reconstruction can be derived:

$$\begin{bmatrix} a_1(x,y) \\ b_1(x,y) \end{bmatrix} = \begin{bmatrix} e^{i\varphi_1} & e^{i(\varphi_1+\Delta\varphi)} \\ e^{-i\varphi_1} & e^{-i(\varphi_1+\Delta\varphi)} \end{bmatrix} \begin{bmatrix} \rho(x,y) \\ \rho(x,y - FOV/2) \end{bmatrix}, \quad [A1]$$

with a_1 and b_1 being pixel intensities of actual and virtual image, respectively. The matrix $E^H E$ in the g -factor from Eq. [9] is given by:

$$E^H E = \begin{bmatrix} 2 & e^{2i\varphi_1} + e^{2i(\varphi_1+\Delta\varphi)} \\ e^{-2i\varphi_1} + e^{-2i(\varphi_1+\Delta\varphi)} & 2 \end{bmatrix} \quad [A2]$$

and its inverse can be written as:

$$(E^H E)^{-1} = \frac{1}{2 - e^{2i\Delta\varphi} - e^{-2i\Delta\varphi}} \times \begin{bmatrix} 2 & -e^{2i\varphi_1} - e^{2i(\varphi_1+\Delta\varphi)} \\ -e^{-2i\varphi_1} - e^{-2i(\varphi_1+\Delta\varphi)} & 2 \end{bmatrix}. \quad [A3]$$

Hence, the g -factor $g_i = \sqrt{((E^H E)^{-1})_{i,i} (E^H E)_{i,i}}$ for a pixel i is given by:

$$g_i = \sqrt{\frac{4}{2 - e^{2i\Delta\varphi} - e^{-2i\Delta\varphi}}} = \sqrt{\frac{4}{2 - 2\cos(2\Delta\varphi)}} = \sqrt{\frac{2}{2(\sin(\Delta\varphi))^2}} = \frac{1}{\sin(\Delta\varphi)}, \quad [A4]$$

using the trigonometric relationships $\cos z = \frac{1}{2}(e^{iz} + e^{-iz})$ and $\cos(2z) = 1 - 2(\sin(z))^2$.

Thus, the noise enhancement due to the g -factor is determined only by the phase difference between the superimposed pixels. For imaging setups using multiple coils and undersampling rates $R > 2$, an analytical expression for the g -factor gets more complicated.

REFERENCES

1. Noll DC, Nishimura DG, Macovski A. Homodyne detection in magnetic resonance imaging. *IEEE Trans Med Imaging* 1991;10:154–163.
2. Liang ZP, Boada FE, Constable RT, Haacke EM, Lauterbur PC, Smith MR. Constrained reconstruction methods in MR imaging. *Rev Magn Reson Med* 1992;4:67–185.
3. McGibney G, Smith MR, Nichols ST, Crawley A. Quantitative evaluation of several partial Fourier reconstruction algorithms used in MRI. *Magn Reson Med* 1993;30:51–59.
4. Sodickson DK, Manning WJ. Simultaneous acquisition of spatial harmonics (SMASH): fast imaging with radiofrequency coil arrays. *Magn Reson Med* 1997;38:591–603.
5. Pruessmann KP, Weiger M, Scheidegger MB, Boesiger P. SENSE: sensitivity encoding for fast MRI. *Magn Reson Med* 1999;42:952–962.
6. Griswold MA, Jakob PM, Heidemann RM, Nittka M, Jellus V, Wang J, Kiefer B, Haase A. Generalized autocalibrating partially parallel acquisitions (GRAPPA). *Magn Reson Med* 2002;47:1202–1210.
7. Griswold MA, Jakob PM, Chen Q, Goldfarb JW, Manning WJ, Edelman RR, Sodickson DK. Resolution enhancement in single-shot imaging using simultaneous acquisition of spatial harmonics (SMASH). *Magn Reson Med* 1999;41:1236–1245.
8. King KF, Angelos L. SENSE with partial Fourier homodyne reconstruction. In: *Proc 8th Scientific Meeting ISMRM*, Denver, CO; 2000. p 153.
9. Heidemann RM, Griswold MA, Kiefer B, Nittka M, Wang J, Jellus V, Jakob PM. Resolution enhancement in lung 1H imaging using parallel imaging methods. *Magn Reson Med* 2003;49:391–394.
10. Klarhöfer M, Dilharreguy B, van Gelderen P, Moonen CT. A PRESTO-SENSE sequence with alternating partial-Fourier encoding for rapid susceptibility-weighted 3D MRI time series. *Magn Reson Med* 2003;50: 830–838.

11. Bydder M, Robson MD. Partial fourier partially parallel imaging. *Magn Reson Med* 2005;53:1393–1401.
12. Samsonov A, Kholmovski E, Johnson C. Phase-constrained reconstruction of sensitivity-encoded MRI Data with POCSENSE. In: Proc 11th Scientific Meeting ISMRM, Kyoto, Japan; 2004. p 2647.
13. Lew C, Spielman D, Bammer R. TurboSENSE: phase estimation in temporal phase-constrained parallel imaging. In: Proc 11th Scientific Meeting ISMRM, Kyoto, Japan; 2004. p 2646.
14. Willig-Onwuachi JD, Yeh EN, Grant AK, Ohliger MA, McKenzie CA, Sodickson DK. Phase-constrained parallel MR image reconstruction. *J Magn Reson* 2005;176:187–198.
15. Hajnal JV, Larkman DJ, Herlihy DJ. An array that exploits phase for SENSE imaging. In: Proc 8th Scientific Meeting ISMRM, Denver, CO; 2000. p 1719.
16. Griswold MA. Advanced k-space techniques. In: Proc 2nd International Workshop on Parallel MRI, Zurich, Switzerland; 2004. p 16.
17. Qu P, Shen GX, Wang C, Wu B, Yuan J. Tailored utilization of acquired k-space points for GRAPPA reconstruction. *J Magn Reson* 2005;174:60–67.
18. Wang Z, Wang J, Detre JA. Improved data reconstruction method for GRAPPA. *Magn Reson Med* 2005;54:738–742 [Erratum: *Magn Reson Med* 2006;56:234].
19. Nana R, Zhao T, Hu X. Automatic kernel selection for optimal GRAPPA reconstruction. In: Proc Scientific Meeting ISMRM, Berlin, Germany; 2007. p 747.
20. Samsonov AA, Block WF. On optimality of parallel MRI in k-space. In: Proc Scientific Meeting ISMRM, Berlin, Germany; 2007. p 743.
21. Madore B, Glover GH, Pelc NJ. Unaliasing by fourier-encoding the overlaps using the temporal dimension (UNFOLD), applied to cardiac imaging and fMRI. *Magn Reson Med* 1999;42:813–828.
22. Kellman P, Epstein FH, McVeigh ER. Adaptive sensitivity encoding incorporating temporal filtering (TSENSE). *Magn Reson Med* 2001;45:846–852.
23. Breuer FA, Kellman P, Griswold MA, Jakob PM. Dynamic autocalibrated parallel imaging using temporal GRAPPA (TGRAPPA). *Magn Reson Med* 2005;53:981–985.
24. Köstler H, Sandstede JJ, Lipke C, Landschutz W, Beer M, Hahn D. Auto-SENSE perfusion imaging of the whole human heart. *J Magn Reson Imaging* 2003;18:702–708.
25. Walsh DO, Gmitro AF, Marcellin MW. Adaptive reconstruction of phased array MR imagery. *Magn Reson Med* 2000;43:682–690.
26. Lagarias JC, Reeds JA, Wright MH, Wright PE. Convergence properties of the Nelder-Mead simplex method in low dimensions. *SIAM J Optim* 1998;9:112–147.